Proceedings of the ASME 2010 3rd Joint US-European Fluids Engineering Summer Meeting and 8th International Conference on Nanochannels, Microchannels, and Minichannels
FEDSM-ICNMM2010
August 1-5, 2010, Montreal, Canada

FEDSM-ICNMM2010-30869

TESTING AND ANALYSIS OF AN OSCILLATING HYDROFOILS TURBINE CONCEPT

Thomas Kinsey
Department of Mechanical Engineering
Laval University
Quebec City, Quebec G1V 0A6
Canada
Email: thomas.kinsey.1@ulaval.ca

Guy Dumas
Department of Mechanical Engineering
Laval University
Quebec City, Quebec G1V 0A6
Canada
Email: gdumas@gmc.ulaval.ca

ABSTRACT

A new concept of hydrokinetic turbine using oscillating hydrofoils to extract energy from water currents (tidal or gravitational) is presented, tested and analyzed in the present investigation. Due to its rectangular extraction plane, this technology is particularly well suited for river beds and shallow waters near the coasts. The present turbine is a 2 kW prototype, composed of two rectangular oscillating hydrofoils of aspect ratio 7 in a tandem spatial configuration. The pitching motion of each hydrofoil is coupled to their cyclic heaving motion through four-link mechanisms which effectively yield a one-degree-of-freedom system driving a speed-controlled electric generator. The turbine has been mounted on a custom-made pontoon boat and dragged on a lake at different velocities. Instantaneous extracted power has been measured and cycle-averaged for several water flow velocities and hydrofoil oscillation frequencies. Results are demonstrated to be self-consistent and validate our extensive 2D flow simulation database. The present data show optimal performances of the oscillating hydrofoils concept at a reduced frequency of about 0.12, at which condition the measured power extraction efficiency reaches 40% once the overall losses in the mechanical system are taken into account. Further measurements of power extraction with a single oscillating hydrofoil have also been performed by taking out the downstream hydrofoil of the tandem pair. Those measurements favorably compare, quantitatively, with available 3D CFD predictions. The 40% hydrodynamic efficiency of this first prototype exceeds expectation and reaches levels comparable to the best performances achievable with modern rotor-blades turbines. It thus demonstrates the promising potential of the oscillating hydrofoils technology to efficiently extract power from an incoming water flow.

INTRODUCTION

The international commitment to reduce our dependency on fossil fuels has motivated significant research efforts in recent years on alternative energy sources that are clean and renewable. Wind and solar energy are well known examples, to which one can now add the huge amount of kinetic energy available in rivers and tidal flows. Indeed, the prospect of harnessing water flow energy with hydrokinetic turbines is becoming more attractive than ever among renewable energies, mainly due to the high energy density of flowing water, to its good predictability and its minimal environmental and human impact expected once deployed on the seabed.

The hydrokinetic turbines sector is growing fast with several new concepts and prototypes being developed in many countries. Most of them are using horizontal axis rotor blades (as most modern wind turbines) or vertical axis rotor blades (as Darrieus-type wind turbines). Other designs have also been proposed [1–3].

The use of oscillating rectangular lifting surfaces (hydrofoils) is an interesting alternative to rotating blades turbine. The concept offers an obvious advantage in shallow water sites due to its rectangular extraction plane, allowing the possibility to scale up the rated power by simply increasing the turbine hydrofoil

Copyright © 2010 by ASME

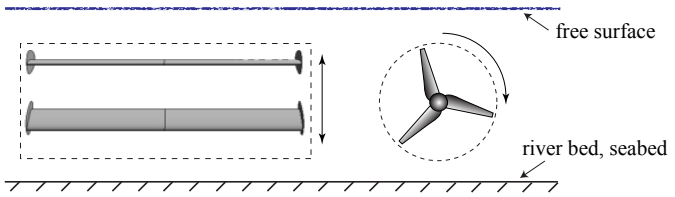

FIGURE 1. FRONT VIEW OF THE RECTANGULAR EXTRACTION PLANE OF THE OSCILLATING HYDROFOILS TURBINE COMPARED TO THE CLASSICAL ROTOR BLADE DESIGN.

span (see Fig. 1). Furthermore, the untwisted hydrofoils in the oscillating concept have a much simpler geometry and are easier to produce than usual rotor blades. This is the concept examined and tested in this study. There has been only a few investigations and demonstrations carried out on this subject over its brief history of about 30 years. Before surveying those contributions, let us first describe formally the motion of each hydrofoil involved here.

The oscillating hydrofoil motion hereafter considered (see Fig. 2) is a combined heave-pitch motion that, restricting to a pitching axis located on the chord line at position x_p from the leading edge, is expressed as:

$$\theta(t) = \theta_0 \sin(\gamma t) \tag{1}$$

$$h(t) = H_0 \sin(\gamma t + \phi) \tag{2}$$

where θ_0 and H_0 are respectively the pitching and heaving amplitudes, γ the angular frequency ($= 2\pi f$), and ϕ is the phase difference between the two motions.

In 1981, McKinney and DeLaurier [4] reported the first use of oscillating wings to extract power from a fluid flow. Their prototype, the "Wingmill" extracted energy from an air flow. They investigated mainly the effect of the phase angle between the pitching and the heaving contributions to the oscillating motion (referred to as motion phase). They showed that maximum power extraction occurs at a phase angle of 110° while maximum efficiency is achieved for a phase angle of 90°. Their 90 W wind tunnel prototype reached a maximal power extraction efficiency of 16.8%, which was considered satisfactory at the time, for a pitching amplitude of 30 degrees, a heaving amplitude of 0.3 chord length and a reduced frequency of 0.12.

More recently, numerical studies (panel-code and Navier-Stokes simulations) as well as some rather unsuccessful water channel experiments were performed at Monterey-based Naval Postgraduate School in California [5] . Their URANS simulations of a single oscillating airfoil predicted high efficiency, nearly 40%, for cases undergoing well-synchronized dynamic stall.

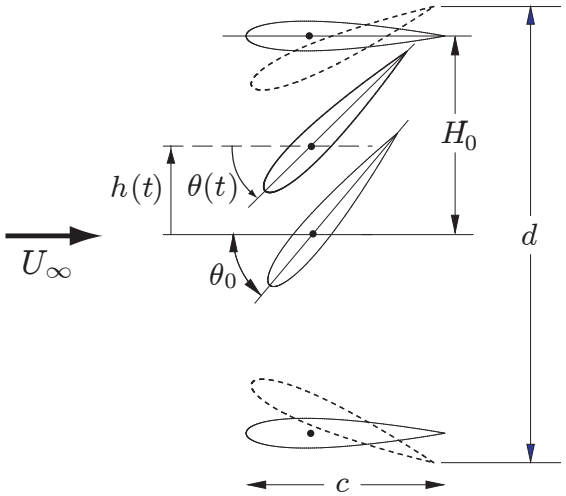

FIGURE 2. HEAVING AND PITCHING MOTIONS ($\phi = 90°$). $d = 2.55\,c$ WHEN $H_0 = c$ AND $\theta_0 = 75°$.

The first commercial prototype of an oscillating-hydrofoil hydrokinetic turbine is the 150 kW "Stingray" prototype from the Engineering Business Ltd [6–9]. The "Stingray" design consisted of a single hydrofoil and was tested in 2003 in Scotland. Unfortunately it was tagged non economically viable following poor results. It reached a maximal production of 85 kW for a modest power extraction efficiency of 11.5%.

Currently, the company Pulse Tidal Ltd. is testing a dual-hydrofoils 100 kW turbine in the UK [10]. Their prototype uses two hydrofoils in a tandem configuration.

Since 2003, research on oscillating-wings aerodynamics aiming at power extraction applications has been performed at Laval University computational fluid dynamics laboratory (LMFN). Extensive numerical simulations [11–14] have led the way to the HAO research project (Hydrolienne à Ailes Oscillantes: Oscillating-hydrofoils hydrokinetic turbine), started in 2006, and involving the development and field testing of a 2 kW turbine prototype. The main purpose of the experimental campaign that has taken place during the summer and fall of 2009 at Lac Beauport near Quebec City was to assert the actual energy extraction potential of the oscillating-hydrofoils turbine technology [1]. The experimental results were also sought to help validate and improve the numerical models.

This paper describes the prototype tested, the instruments and experimental protocols and the results obtained. Furthermore, comparisons with CFD predictions are provided, in 2D for the single hydrofoil and the tandem configuration, and in 3D for the single hydrofoil with endplates, once a brief description of

[1] Project website: http://hydrolienne.fsg.ulaval.ca/en

Copyright © 2010 by ASME

the numerical approach and the URANS model has been presented.

EXPERIMENTAL SETUP

The experimental rig, thoroughly detailed in [15], includes an oscillating-hydrofoils hydrokinetic turbine mounted on a custom-made pontoon boat driven by an outboard motor as shown in Fig. 3. Both the pontoon boat and the hydrokinetic turbine have been designed and built at Laval University's Department of Mechanical Engineering.

The boat has two floats made from rows of empty plastic barrels encapsulated in an aluminum frame. The barrels provide the needed buoyancy in addition to allowing the possibility to level off the boat by filling part of them with water. The middle section of the pontoon consists of two compartments apart from an open center dedicated to the turbine. A lift structure fixed to the boat allows to raise the turbine for transit or to lower it down 2m deep for operation.

The turbine itself consists of a one degree of freedom dual hydrofoils system. The hydrofoils are mechanically coupled to a rotating shaft as shown in Fig. 4. Two aluminum rods (parts a) are connected on one end to the hydrofoils pivoting rod and at the other end to the rotating shaft via a crankshaft (parts b). This is equivalent to a duplicated four-link mechanism which allows both hydrofoils to heave (approximating the actual circle arc motion to a straight vertical displacement). Two more four-link mechanisms are required to account for the pitching motion of the hydrofoils (parts c). The pitching motion necessitates three sprockets and two chains per hydrofoil (parts d). In this figure, the pitching mechanism on the left is connected through a chain to the downstream hydrofoil pitching axis, while the right pitching mechanism is linked to the upstream hydrofoil. These mechanisms are shifted 180 degrees in accordance with the pitching phase between hydrofoils.

The relative lengths of the rods part of the four-link mechanisms have been carefully chosen in order to approximate closely the motion described in Eqns. 1 and 2 when the rotating shaft is turning at constant speed.

The rotating shaft is connected to the mechanical/electrical conversion group as shown in Fig. 3. The conversion group includes an helicoidal 20:1 gearbox (Boston Gear 652B-20), a 46 kg flywheel and a generator (DC motor, Baldor CDP-3605). With all the equipment on board, the total weight of the boat is approximately 2 000 kg.

The generator rotational speed is controlled during a run via a DRU-R60/200R Elmo drive powered by a 180 volts (1.8 kW.h) battery bank (15x B.B. battery 12V/10Ah, BP10-12). The angular speed reference for the electrical drive is given by a resolver (AMCI H25-FS-R5B) mounted on the low-speed far-end side of the shaft. The electrical power produced by the generator is recharging the battery bank. Once the batteries are fully charged, a chopper circuit dumps the excess electricity through resistances where it is dissipated in heat.

TABLE 1. HYDROKINETIC TURBINE PARAMETRIC DETAILS.

hydrofoils section	NACA 0015
chord length (c)	0.24 m
span (b)	1.68 m
pitching axis (x_p)	$c/3$
heaving amplitude (H_0)	c
pitching amplitude (θ_0)	75°
inter-wing phase shift (ϕ_{1-2})	180°
motion phase (ϕ)	90°
inter-wing spacing (L_x)	$5.4\,c$

Turbine Details

In the current experimental configuration, the oscillating hydrofoils adopt a tandem spatial configuration (see Fig. 3). Motion amplitudes, phase shifts and inter-wing spacing are fixed based on optimal results from 2D URANS CFD simulations [11–14]. These parameters, as well as the hydrofoils size are summarized in Table 1 and Fig. 5 which also shows that endplates are used on each hydrofoil in order to limit 3D hydrodynamic losses.

During the field tests, the flow velocity U (through the boat speed) and the hydrofoils oscillation frequency f were varied between runs in order to cover the targeted range of reduced frequency f^* which is defined as:

$$f^* = \frac{f\,c}{U} \tag{3}$$

The nominal operating conditions correspond here to an upstream water velocity of $U = 2$ m/s and a turbine oscillation frequency of $f = 1.0$ Hz which yield a reduced frequency of $f^* = 0.12$.

Copyright © 2010 by ASME

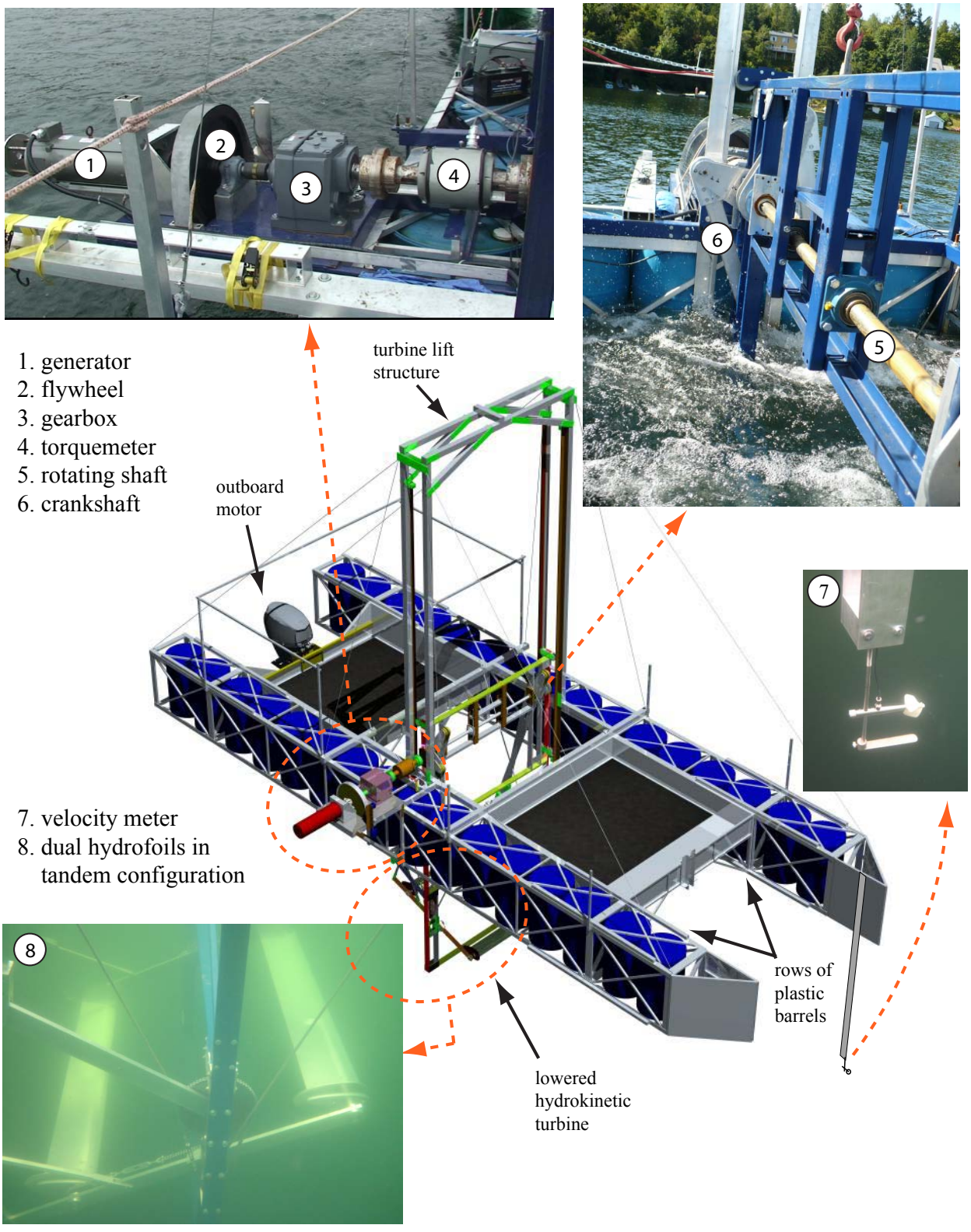

FIGURE 3. SCHEMATIC OF THE COMPLETE EXPERIMENTAL SETUP (PONTOON BOAT AND MOUNTED TURBINE).

Copyright © 2010 by ASME

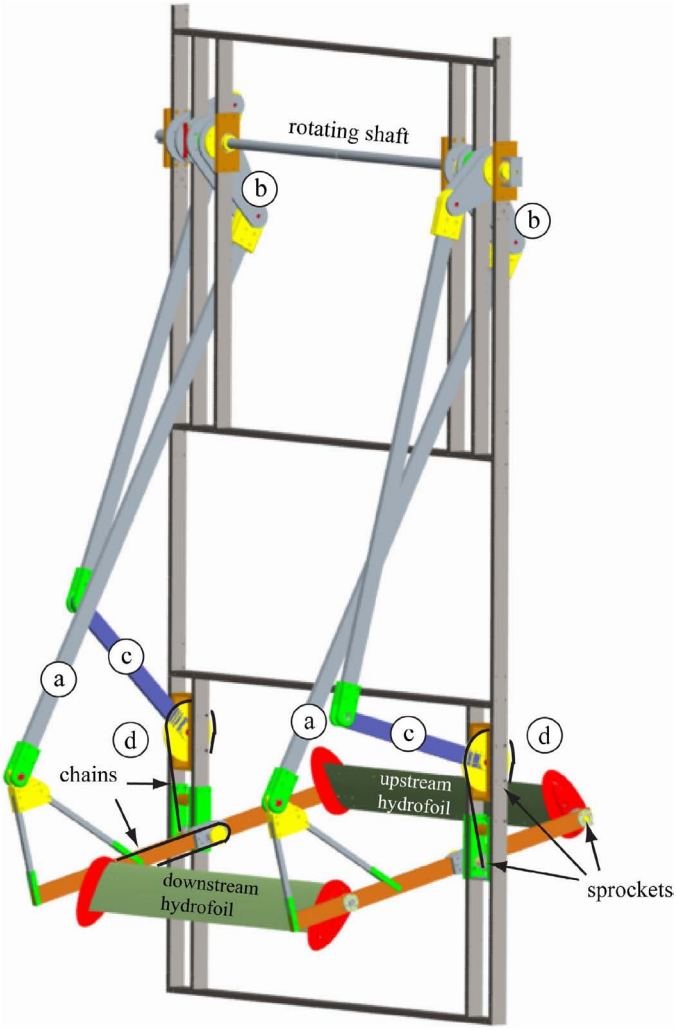

FIGURE 4. SCHEMATIC OF THE HYDROKINETIC TURBINE MECHANISMS ALLOWING THE COUPLING OF THE HYDROFOILS OSCILLATING MOTION TO A ROTATING SHAFT.

INSTRUMENTATION

Hardware

The instantaneous torque on the rotating shaft is measured through a torquemeter (BLH Type A-12, part 4 on Fig. 3) located on the rotating shaft between the turbine and the gearbox. The torquemeter signal is amplified through a strain gage amplifier (Vishay Measurements Group P-3500 strain indicator). A velocity probe (C2 OTT velocity meter, part 7) is used underwater to measure the water flow velocity. Two 3-axis accelerometers are fixed to the boat in order to assert and quantify its stability once in motion.

The shaft angular speed is measured using an emulated encoder signal generated by the electrical drive based on the resolver signal. This signal is treated by a digital signal processor (DSP) into a 0-5 volts ramp for every shaft revolution. These analog ramps are then acquired at 1000 Hz together with the torque, velocity probe and accelerometers signals through an acquisition card (National Instruments DAQCard-6062E 12bit A/N) connected to a laptop computer (Toshiba Tecra Pentium M, 1.4GHz).

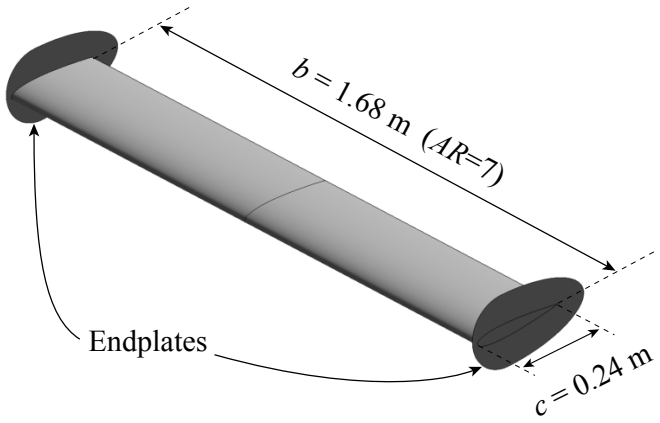

FIGURE 5. HYDROFOIL DETAILS.

Data Processing

The velocity meter probe used produces a square wave signal whose period coincides with one revolution of its rotor. The signal frequency is proportional to the water flow velocity via its scaling law. To remove occasional spurious data points in the wavefront neighborhood, the square wave signal is processed point-to-point. This operation leads to a computed water velocity curve necessitating no further filtering.

The instantaneous shaft angular velocity is filtered using a low-pass 10 Hz spectral filter specifically designed to induce no data phase shift. The same filter is applied to accelerometers data, higher frequencies vibrations being of no interest to assert the pontoon boat stability.

The torque signal has a low noise level and does not require filtering prior to the phase-averaged operation (described below).

A typical run, at a given oscillation frequency f and water flow velocity U, lasts 1-2 minutes and includes 50 to 100 turbine oscillation cycles. The acquired signals are subdivided into oscillation cycles using the encoder index occurrence. Cycle-averaged values of water flow velocity and oscillation frequency are then computed. Once these values are well stabilized from cycle to cycle, 10 to 40 consecutive cycles are chosen and phase-averaged. This results in a phase-averaged instantaneous signal over one period of oscillation for every type of measurement performed. This operation has turned out much simpler than antici-

Copyright © 2010 by ASME

pated due to the excellent repeatability of the experimental measurements.

The power extracted by the turbine is measured at the low-speed side shaft as the product of the instantaneous torque $\mathscr{T}$ and angular velocity Ω.

$$P(t) = \mathscr{T}(t)\,\Omega(t) \tag{4}$$

The total power available (P_a) in the water flow through the extraction plane is given by the following relation:

$$P_a = \frac{1}{2}\rho\,\overline{U}^3\,b\,d \tag{5}$$

where ρ is the water density ($\rho = 999$ kg/m^3), b is the hydrofoil span, $\overline{U}$ is the cycle-averaged flow velocity measured by the velocity meter and d is the overall extent of the hydrofoil vertical motion (Fig. 2) which is function of H_0 and θ_0 (for $H_0 = c$ and $\theta_0 = 75°$, $d = 2.55\,c$).

The efficiency η is defined as the ratio of the cycle-averaged power extracted ($\overline{P}$) to the total power available:

$$\eta = \frac{\overline{P}}{P_a} \tag{6}$$

The torque and angular velocity being measured directly on the low speed shaft, the extracted power calculated in Eqn. 4 corresponds to the hydrodynamic power extraction minus the mechanical losses in the system up to the torquemeter, which is located just before the gearbox on the transmission shaft (see Fig. 3).

The efficiency calculated by Eqn. 6 may then be qualified as a "water-to-gearbox efficiency". To get the "water-to-wire" efficiency, one should further take into account losses in the gearbox and the generator, by a measure of the electrical power at the generator output. This has not been done during the present experimental campaign, the focus being to get a power measurement as close as possible to the turbine itself to be able to adequately estimate its hydrodynamic efficiency η_{hydro}.

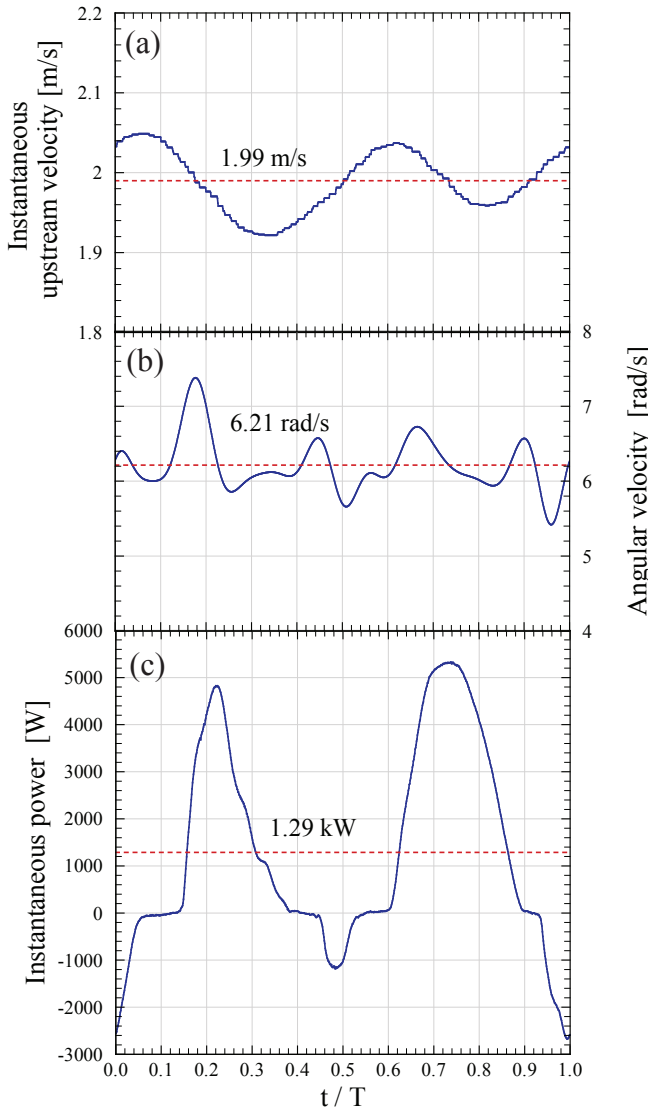

FIGURE 6. TYPICAL INSTANTANEOUS MEASUREMENT CURVES OVER ONE CYCLE; (a) UPSTREAM VELOCITY (BOAT SPEED), (b) ANGULAR VELOCITY OF THE LOW-SPEED SIDE OF THE ROTATING SHAFT AND (c) POWER MEASURED AT THE TORQUEMETER.

RESULTS

Instantaneous and Cycle-Averaged Data

During each test, probes and sensors data are acquired at a rate of 1000 Hz. This allows calculation of the cyclic instantaneous power curve from the product of torque and angular velocity (Eqn. 4). Typical instantaneous curves are shown in Fig. 6.

From the instantaneous power curve (Fig. 6c), one notes large fluctuations of power over one cycle, from -2.7 to 5.4 kW, leading to a cycle-averaged value of 1.29 kW of extracted power for this particular case. The large fluctuations are basically due to the 180 degrees phase between the two hydrofoils; both hydrofoils are reaching their peak production at the same time. Of course, a commercial implementation of this turbine concept should rely on the use of several phase-shifted hydrofoils units to achieve a more uniform power production.

Figure 6a shows the evolution of the upstream flow velocity over one cycle (which, in the present setup, is equivalent to

Copyright © 2010 by ASME

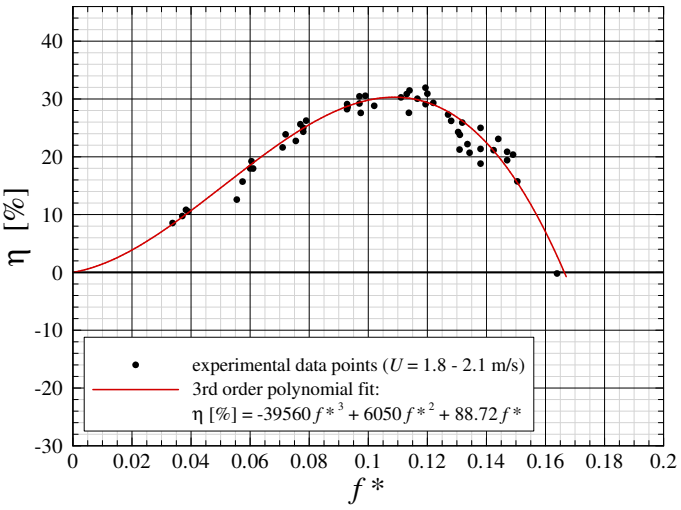

FIGURE 7. POWER EXTRACTION EFFICIENCY VERSUS REDUCED FREQUENCY FOR DUAL-HYDROFOIL TESTING. EXPERIMENTAL DATA POINTS SHOWN CORRESPOND TO RUNS WITH A MEAN UPSTREAM FLOW VELOCITY RANGING FROM 1.8 TO 2.0 m/s. AVERAGE ERROR IS $\pm 2.3\%$ (ABSOLUTE) ON η AND ± 0.002 ON f^*.

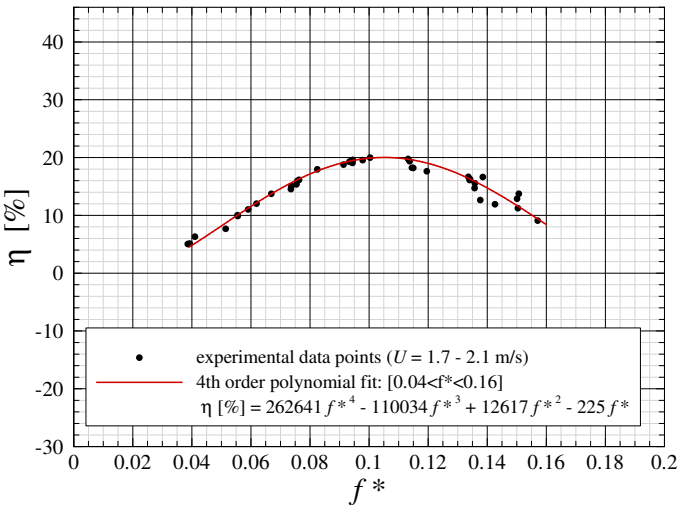

FIGURE 8. POWER EXTRACTION EFFICIENCY VERSUS REDUCED FREQUENCY FOR SINGLE-HYDROFOIL TESTING. EXPERIMENTAL DATA POINTS SHOWN CORRESPOND TO RUNS WITH A MEAN UPSTREAM FLOW VELOCITY RANGING FROM 1.7 TO 2.0 m/s. AVERAGE ERROR IS $\pm 1.7\%$ (ABSOLUTE) ON η AND ± 0.002 ON f^*.

the boat speed). Fluctuations of about 3% are observed on both sides of the cycle-averaged value of 1.99 m/s. These velocity fluctuations are mostly due to the large variations of drag forces on the turbine over one cycle. This is consistent with onboard accelerometers measurements which indicate a forward acceleration in agreement with the velocity variations measured with the velocity meter. The capacity to maintain the boat speed reasonably constant is possible due to its large inertia. Furthermore, even if the turbine drag varies greatly, it occurs over one oscillation cycle whose time period is too short (about 1s) to affect significantly the boat stability and speed.

The rotating shaft angular velocity is indirectly controlled through torque control by the electrical drive, in order to maintain a constant angular velocity. This speed control is imperfect as can be seen in Fig. 6b. Rotating velocity fluctuations reach 19% above and 13% below the cycle-averaged value in this particular case. Most of our experimental runs present instantaneous angular velocity variations ranging from 10% to 30%.

Field tests results concerning the power extraction efficiency versus reduced frequency for the complete hydrokinetic turbine (two hydrofoils in tandem configuration) are shown on Fig. 7.

One observes water-to-gearbox efficiency reaching up to 30% for reduced frequencies in the range of 0.10 to 0.12 (see Eqn. 3).

Single Hydrofoil Results

Further tests were performed with the downstream hydrofoil removed. The purpose of these single-hydrofoil field tests is to discriminate between each hydrofoil contribution to the power extracted.

Results in terms of power extraction efficiency versus reduced frequency for the single-hydrofoil hydrokinetic turbine are shown on Fig. 8.

This time, one observes a water-to-gearbox efficiency reaching 20% at a reduced frequency of about $f^* = 0.11$.

It is now possible to compare these single-hydrofoil results (Fig. 8) with those related to the dual hydrofoils in tandem configuration (Fig. 7). In both cases, the turbine reaches its peak efficiency for a reduced frequency near 0.11. Based on the single hydrofoil results, one thus infers that in the case of the complete turbine, the upstream hydrofoil contributes up to 2/3 of the total power extracted leaving only 1/3 contribution to the downstream hydrofoil.

Mechanical Losses Estimates

As previously mentioned, the power extracted is computed from the torque measured on the low speed side of the gearbox and the shaft angular velocity. This measurement equals the power extracted from the water flow by the oscillating hydrofoils minus the mechanical losses in the system up to the gearbox. These losses are associated to the dynamic mechanical friction

Copyright © 2010 by ASME

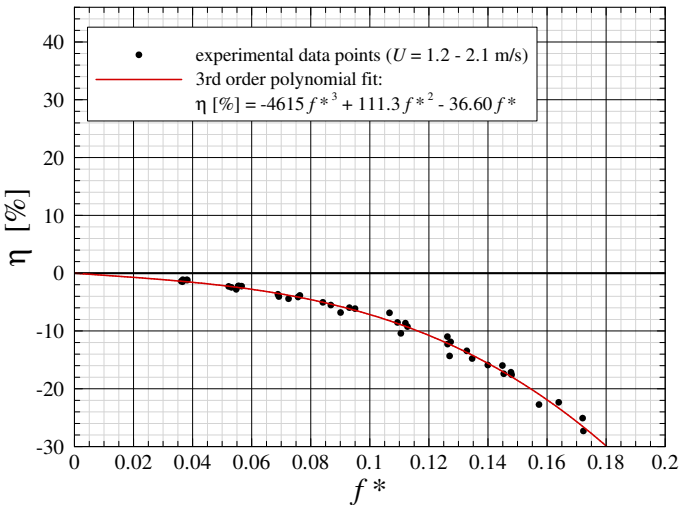

FIGURE 9. POWER EXTRACTION EFFICIENCY VERSUS REDUCED FREQUENCY FOR TESTS WITH NO HYDROFOIL. AVERAGE ERROR IS $\pm 1.1\%$ (ABSOLUTE) ON η AND ± 0.002 ON f^*.

and, mostly, to the power needed to move the long heaving and pitching rods through the water flow.

A good estimate of these losses is the power needed to move the hydrofoil-less turbine through the water flow. To address this point, both hydrofoils were removed and the system driven at different frequencies in different upstream flow velocities. To allow direct comparison with previous results, Fig. 9 shows the data plotted in terms of power extraction efficiency to reduced frequency. As expected, efficiency values are negative (in these cases without hydrofoils) and show that more power is required to drive the system through the water flow as frequency is increased.

Note that even if the operating conditions are similar, loads will be minimal on the bearings for the runs without hydrofoils compared to the full turbine runs. Therefore, one expects to underestimate mechanical friction losses in the system. The losses estimates provided by runs without hydrofoils are thus considered as a minimal bound for the actual mechanical losses which will be considered in section 6 where hydrodynamic efficiency is addressed together with comparisons with CFD predictions.

NUMERICS

The finite-volumes commercial code Ansys Fluent [16] is used to solve the Unsteady-Reynolds-Averaged-Navier-Stokes (URANS) equations about the hydrofoils. The procedure is essentially the one used for the parametric study presented in [11] for low-Reynolds oscillating wings. However the current high-Reynolds ($Re = 500\,000$) simulations use turbulence model-

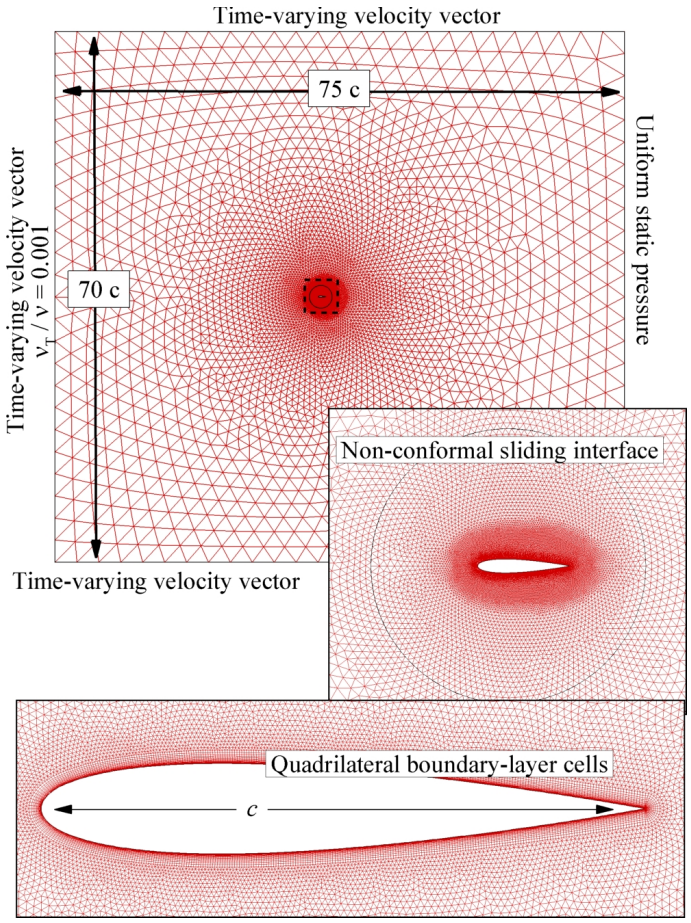

FIGURE 10. 2D URANS MESH DETAILS FOR THE SINGLE OSCILLATING HYDROFOIL.

ing (one-equation Spalart-Allmaras model, strain/vorticity-based production). The SIMPLE algorithm is selected for pressure-velocity coupling. Second order schemes are used for pressure, momentum and turbulent viscosity discretization. The unsteady formulation is based on a first order implicit scheme which is imposed from the use of dynamic mesh capabilities. Absolute convergence criteria of 10^{-5} are set for continuity and velocity components while 10^{-4} is used for the turbulent viscosity.

Let us first consider the case of a single oscillating hydrofoil as depicted in Fig. 10. The motion of the foil is prescribed in Fluent through the use of user-defined functions (UDFs) compiled within the solver. Although the dynamic mesh options are activated, no actual remeshing is done during the computation. Instead, the use of a non-conformal sliding interface centered on the hydrofoil pitching center is used to allow relative motion between the hydrofoil near-body mesh zone and the external mesh zone. This accounts for the pitching part of the oscillating motion. The flow computation is then done in the hydrofoil heaving

Copyright © 2010 by ASME

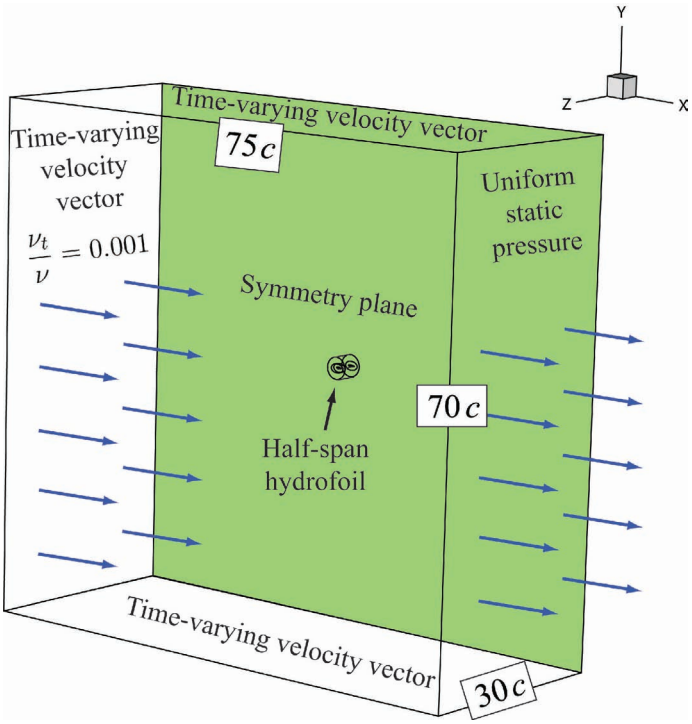

FIGURE 11. DOMAIN SIZE AND BOUNDARY CONDITIONS FOR THE 3D NUMERICAL SIMULATIONS ABOUT THE $AR = 7$ HYDROFOIL EQUIPPED WITH THE SAME ENDPLATES AS ON THE PROTOTYPE.

reference frame. This requires to specify time-varying velocity vectors on the upstream, top and bottom domain boundaries. Furthermore, the reference frame acceleration must be added as a source term to the Navier-Stokes equations. This is again done via user-defined functions. This strategy is summarized in Fig. 10 along with mesh details.

Both 2D and 3D simulations have been performed for cases of a single oscillating hydrofoil. The 2D simulations are carried on until reasonable periodicity is achieved on cycle-averaged values from one cycle to the other (variations of less than 0.1% on cycle-averaged values). This typically requires 5 to 10 oscillation cycles from the impulsive start, depending on the reduced frequency. The time step size is defined as the minimum between 0.5 thousandth oscillation period ($T/2000$) and one hundredth convective time unit ($c/(U_\infty 100)$). The 3D simulations (2,1M cells) each require about 2 weeks to complete on a 16 processors cluster; four simulations have been performed and each of them were run for 3 to 4 oscillation cycles with a time step size of one thousandth oscillation period. Despite the limited number of cycles computed for each case, the periodicity from cycle to cycle was satisfactory at 0.25% for cases associated to $f^* = 0.1, 0.12, 0.14$ and 0.5% for $f^* = 0.2$.

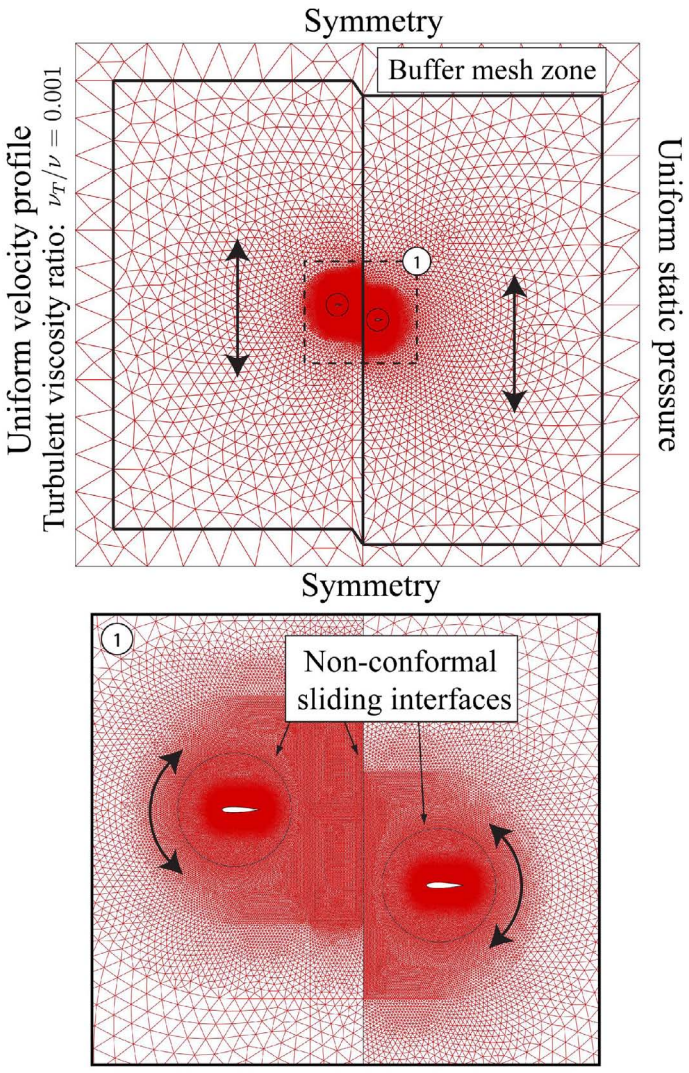

FIGURE 12. THE MESH IS DIVIDED IN 5 DISTINCT MESH ZONES. FOUR OF WHICH ARE MOVING IN RIGID BODY MOTION (EACH HYDROFOIL IS ENCAPSULATED IN A RIGIDLY ROTATING MESH ZONE WHICH IS ITSELF PART OF A LARGE HEAVING MESH ZONE). A BUFFER MESH ZONE IS PRESENT NEAR THE DOMAIN BOUNDARIES IN ORDER TO ALLOW THE HEAVING DEFORMATION OF THE HEAVING MESH ZONES.

The 3D URANS simulations use essentially the same strategy as 2D computations except that the finite hydrofoil symmetry allows to model only half the problem with the use of a symmetry plane right through the hydrofoil mid-span (see Fig. 11). In 3D, the non-conformal sliding interface appears as a closed cylinder surrounding the hydrofoil and its endplate. This cylindrical interface is closed at a half-chord distance farther than the endplate in order to avoid interfaces interpolation to occur right

Copyright © 2010 by ASME

at the wingtip plane. The mesh discretization on the mid-section symmetry plane is the same as the 2D mesh presented in Fig. 10.

For simulations involving two hydrofoils in a tandem configuration, we limit ourselves to 2D modeling, and the strategy must be adapted due to the absence of a common heaving reference frame. Numerical simulations are thus performed in a fixed reference frame. This once again requires the use of dynamic meshes and sliding non-conformal interfaces to allow relative motion of adjacent mesh zones (see Fig. 12). Both hydrofoils are again encapsulated in a circular mesh zone moving in rigid body with them. These circular mesh zones are each surrounded by a large moving mesh zone heaving in rigid body with the hydrofoil. A non-conformal sliding interface allows the relative pitching motion of the hydrofoils and circular mesh zones into the heaving mesh zone. Furthermore, the cells adjacent to the computational domain external boundaries are deforming, playing the role of a buffer mesh zone to allow the heaving cell zones motion. Finally, the hydrofoils motions are phase-shifted so an additional sliding interface is required between the two heaving mesh zones to permit relative motions.

The mesh refinement is done in such a way as to guarantee that the upstream-hydrofoil convected wake stays in a high spatial resolution mesh at all time. This is very important in the present turbine simulations since the downstream hydrofoil interaction with the upstream hydrofoil wake vortices is of great interest.

For each tandem simulation, cycle-averaged values are computed for every oscillation cycle and computation is carried on until periodicity is achieved. To reach periodicity usually requires 5 to 8 cycles.

The instantaneous power $P(t)$ extracted from the flow (per unit depth in the case of 2D computations) by a given hydrofoil comes from the sum of a heaving contribution $P_y(t) = Y(t)V_y(t)$ and a pitching contribution $P_\theta(t) = M(t)\Omega(t)$, where Y is the vertical force on the hydrofoil, V_y the instantaneous heaving velocity, M the resulting torque about the pitching center x_p and Ω the instantaneous pitching velocity. The mean power extracted over one cycle ($\overline{P}$) can then be computed as well as the hydrodynamic efficiency from Eqn. 6.

HYDRODYNAMIC PERFORMANCE PREDICTIONS

In order to compare CFD results with experimental data, mechanical losses in the experimental setup from the turbine itself up to the gearbox (where the power has been measured) must be subtracted in order to get the hydrodynamic efficiency. A minimal bound for the hydrodynamic efficiency is obtained for the single and dual hydrofoils turbine by subtracting to their respective trendlines (Figs. 7 and 8) the mechanical losses estimation provided by runs without hydrofoils (Fig 9).

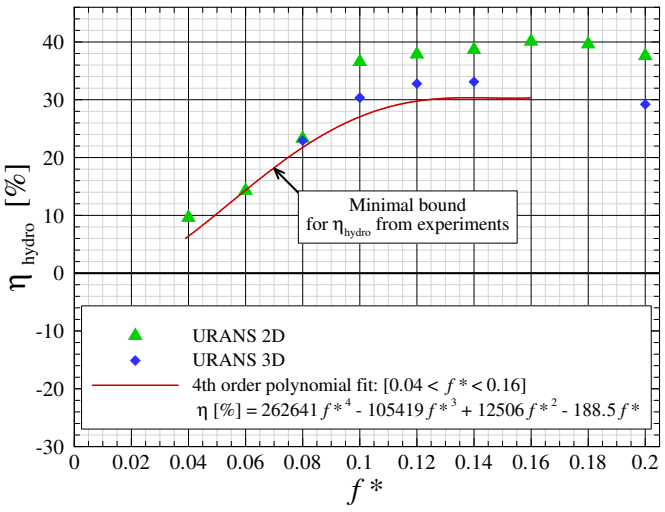

FIGURE 13. COMPARISON BETWEEN 2D AND 3D URANS NUMERICAL RESULTS AND EXPERIMENTAL DATA. HYDRODYNAMIC POWER EXTRACTION EFFICIENCY VERSUS REDUCED FREQUENCY FOR THE SINGLE-HYDROFOIL TURBINE TESTING.

Single Hydrofoil Comparison

For the single hydrofoil case first, this hydrodynamic efficiency estimated from experiments is compared to 2D and 3D CFD results in Fig. 13.

The hydrodynamic efficiency values are found to reach a plateau at $\eta = 30\%$ starting at a reduced frequency of 0.12. CFD results indicate that this plateau is maintained up to about $f^* = 0.20$ (experimental data are available up to $f^* = 0.16$). One thus infers that the drop of efficiency observed in Fig. 8 past $f^* = 0.12$ is mostly due to the increase of mechanical losses with frequency (Fig. 9).

The 2D CFD results match the experimental curve very well for $f^* \leq 0.08$ while they overpredict the actual performances at higher frequencies. It is noted also that the predicted efficiency is more or less constant between $0.10 < f^* < 0.20$.

Whenever available, direct comparisons between 2D and 3D URANS results show the 2D computations overpredicting power extracted by a consistent margin (except for $f^* = 0.08$). The loss of performance due to the finite span ($AR = 7$) represents approximately 15% of the 2D result for the nominal experimental condition at $f^* = 0.12$. One further notes that the 3D simulations predictions compare remarkably well with the estimated experimental minimal hydrodynamic efficiency of a single oscillating hydrofoil.

In terms of flow dynamics, runs related to reduced frequencies below 0.10 experience strong dynamic stall and leading-edge vortex shedding in a bluff-body fashion. At the opposite,

Copyright © 2010 by ASME

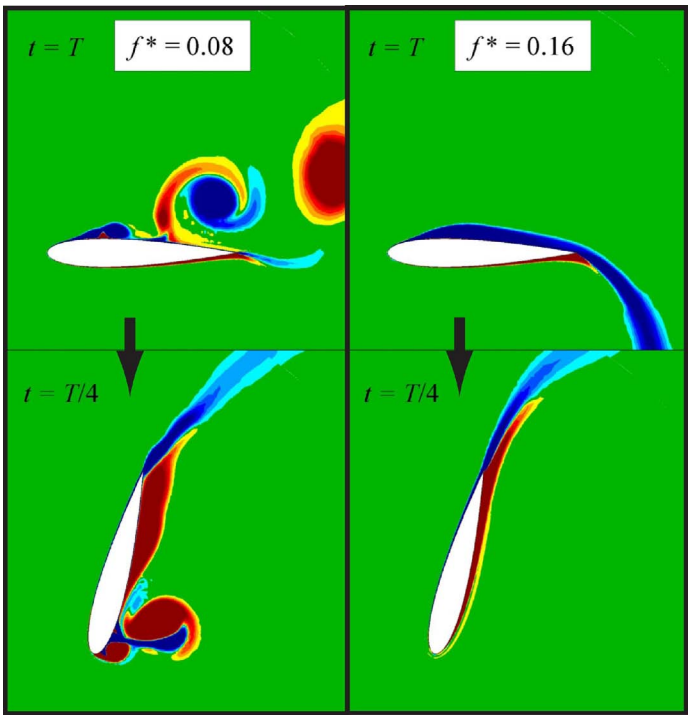

FIGURE 14. ISOSURFACES OF VORTICITY (BLUE FOR NEGATIVE VORTICITY AND RED FOR POSITIVE) AT TWO INSTANTS IN THE HYDROFOIL OSCILLATION CYCLE. AT $f^* = 0.08$ (LEFT), MASSIVE DYNAMIC STALL AND LEADING-EDGE VORTEX SHEDDING OCCURS. AT $f^* = 0.16$ (RIGHT), BOUNDARY LAYERS REMAIN CLOSE TO THE HYDROFOIL AND NO VORTEX SHEDDING OCCURS.

a single hydrofoil oscillating at a reduced frequency of 0.16 and up to at least 0.20 (and of course with amplitudes $H_0 = c$ and $\theta_0 = 75°$) presents essentially no separation. This point is illustrated in Fig. 14 based on the URANS 2D flow fields. The intermediate frequencies ($[0.10 < f^* < 0.14]$) are experiencing dynamic stall vortex shedding, but the leading-edge boundary layer separation is not initiated before $t = T/4$. This leads to a vortex formation which will be shed from the hydrofoil when the latter is around its heaving maxima. Such a timed shedding does not interfere with performance, in opposition to mid-run shedding occurrences at lower frequencies, the peak instantaneous power production being reached at about $t = T/4$ and $t = 3T/4$ when boundary layers are attached.

Classical 3D effects in hydrodynamics of lifting bodies tend to reduce the lift due to the induced downwash. The good agreement observed between 2D predictions and the experimental data at low frequencies suggests that such 3D effects are weak in such cases probably due to the multiple vortex shedding occurrences taking place during each cycle when $f^* < 0.1$. This is further corroborated by a match between 2D and 3D URANS predictions for $f^* = 0.08$ (see Fig.13).

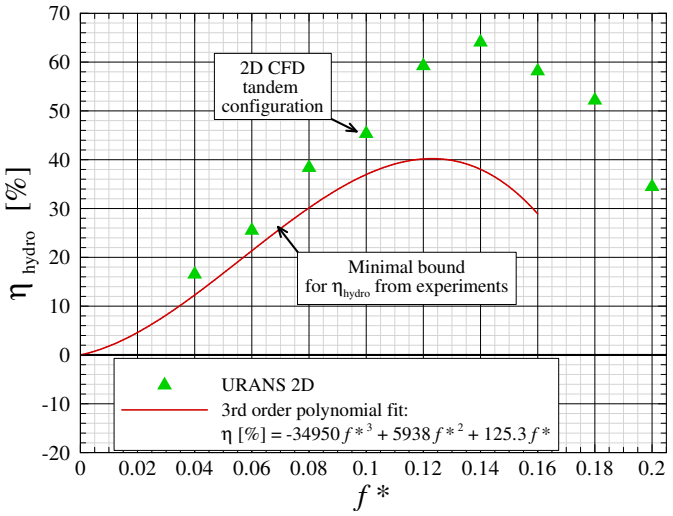

FIGURE 15. ESTIMATED HYDRODYNAMIC POWER EXTRACTION EFFICIENCY VERSUS REDUCED FREQUENCY FOR DUAL-HYDROFOIL TURBINE TESTING.

Tandem Hydrofoils Comparison

In the case of dual hydrofoils, the minimal hydrodynamic efficiencies estimated from experiments is provided as a trendline in Fig. 15. The maximum estimated efficiency is about 40% for a reduced frequency near 0.12. The efficiency drops noticeably past its maximum value. This is due to the fixed inter-wing spacing (L_x) at $5.4c$, which has been chosen (based on CFD modeling) in order to get an optimal downstream hydrofoil power production from a favorable interaction with the upstream hydrofoil wake vortices for a reduced frequency of 0.14 such as illustrated in Fig. 16. At higher frequencies, the downstream hydrofoil positioning is no more optimal. Its mean contribution to power extracted is even falling to zero and eventually to negative values, hindering the turbine global performance.

The capability to vary the inter-wing spacing would allow to maintain good power extraction efficiency on a broader range of reduced frequencies. However, a commercial implementation of this turbine would likely operate with a speed-controlled generator, adjusting the oscillation frequency to the flow velocity in order to operate at a fixed, optimal reduced frequency value.

Comparison with 2D URANS simulations are also provided. The numerical predictions reproduce qualitatively the experimental curve trend but largely overpredict performance for $f^* \geq 0.12$. The total power extracted from the turbine comes from the sum of both hydrofoils contributions. The power contribution of the upstream hydrofoil will be similar here to the results obtained on the single hydrofoil computations (Fig. 13).

Copyright © 2010 by ASME

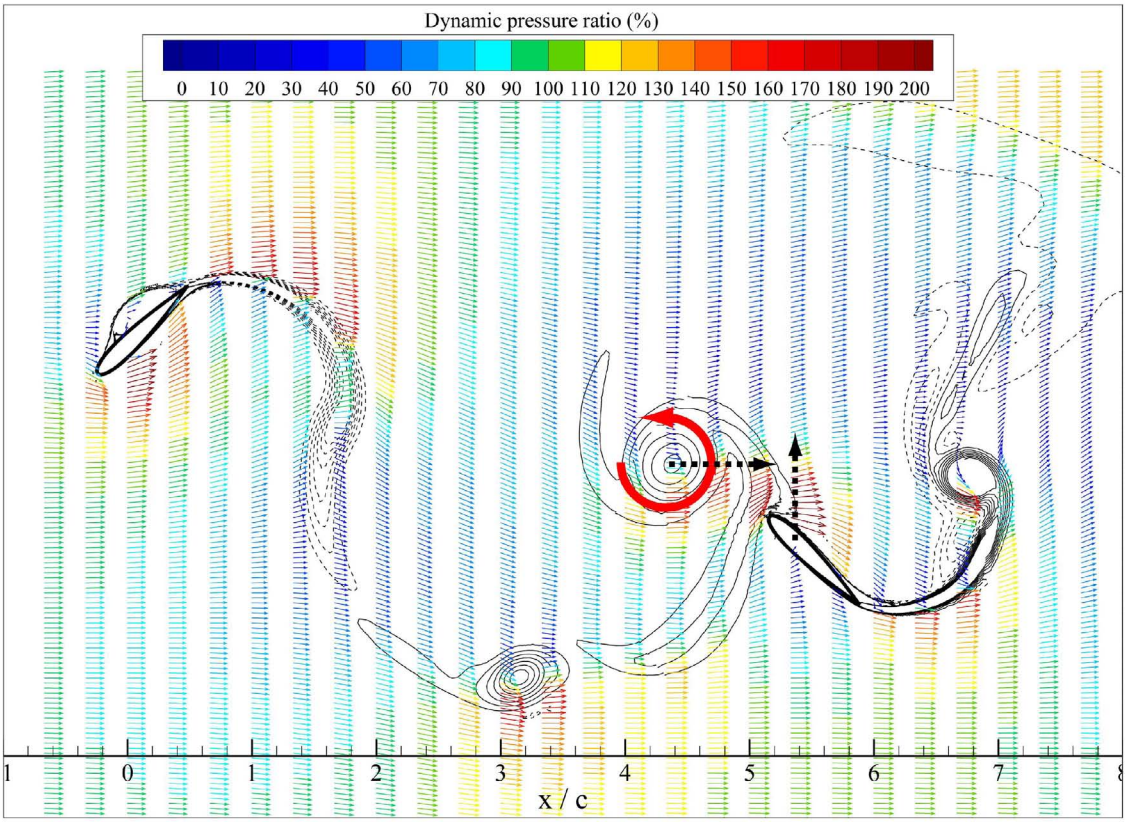

FIGURE 16. EXAMPLE OF ADVANTAGEOUS VORTEX-HYDROFOIL INSTANTANEOUS POSITIONING IN THE CASE $f^* = 0.14$. VELOCITY VECTORS COLORED BY DYNAMIC PRESSURE RATIO $(|V|/U_\infty)^2$ AND ISOLINES OF VORTICITY (DASHED FOR NEGATIVE VORTICITY).

The downstream hydrofoil positioning relative to the upstream hydrofoil has a critical impact on the turbine performance because it operates in the upstream hydrofoil wake. A favorable hydrofoil/wake vortices interaction, as the one presented in Fig. 16, allows to reach efficiencies up to 64% in the 2D CFD simulations.

To predict such high efficiencies may seem surprising at first, considering the classical Betz's law, limiting the hydrodynamic efficiency at 59.3% [17] for a single turbine and to 64.0% [18] for two turbines in a tandem configuration. However, Betz's analysis considers a stationary axisymmetric streamtube of inviscid flow around a turbine. This analysis does not apply to the current oscillating hydrofoils turbine concept due to its strong unsteady character. This is particularly true for the downstream hydrofoil interacting strongly with shed vortices.

It should be noted that the best performance predicted by the 2D URANS computations are characterized by a beneficial strong interaction of the downstream hydrofoil with the upstream hydrofoil wake vortices. However, in the three-dimensional reality, the 2D coherence of the wake vortices will be likely broken (as shown in Fig. 17), resulting in an uncorrelated vortex interaction with the downstream hydrofoil. Thus instantaneous gains due to vortex-induced velocities are unlikely to occur in the 3D reality.

CONCLUSION

A new hydrokinetic turbine prototype has been designed, built and experimentally tested. The turbine relies on the use of two oscillating hydrofoils in a tandem configuration to harness power from the water flow instead of using conventional rotating blades.

This concept is quite promising due to its good hydrodynamic efficiency as well as its rectangular extraction plane which

Copyright © 2010 by ASME

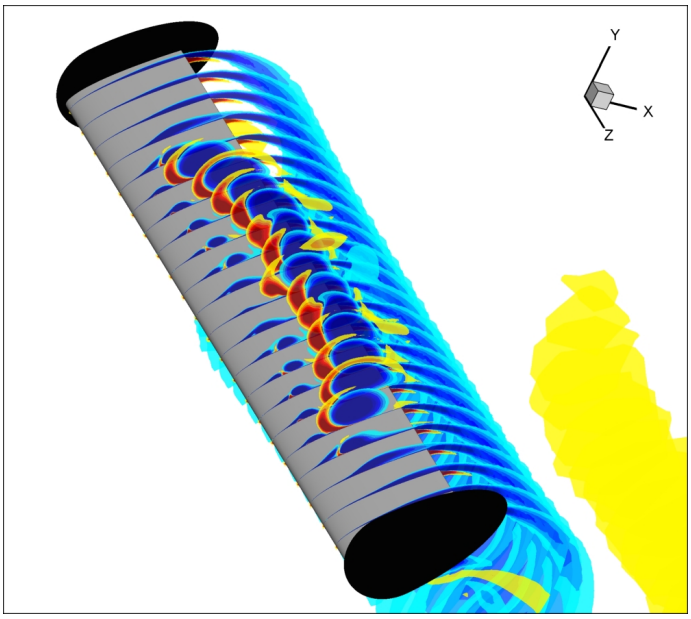

FIGURE 17. EXAMPLE FROM THE 3D URANS SIMULATION OF A 3D VORTEX WITH BROKEN 2D COHERENCE. THE VORTEX SHAPE IS SHOWN USING SLICES SHOWING CONTOURS OF Z-VORTICITY COMPONENT (BLUE FOR NEGATIVE VORTICITY, RED FOR POSITIVE).

is well suited for riverbeds and shallow waters. Its use of untwisted hydrofoils which are less expensive to build than usual twisted rotor blades is also a great asset.

The experimental campaign described in this paper took place on a lake, the hydrokinetic turbine being mounted on a custom-made pontoon boat. This strategy allowed versatility in the choice of the turbine operating conditions and facilitated its deployment.

Results from this campaign show that this prototype, and thus the oscillating hydrofoils concept, presents a good energy extraction potential with performance similar to rotating blades technology. Indeed, the hydrodynamic power extraction efficiency reaches up to 40% for the present dual-hydrofoil turbine in tandem configuration.

Comparisons with 3D URANS numerical simulations show a good agreement on cycle-averaged values predictions for one oscillating hydrofoil. 2D URANS predictions are expected to overpredict the power extracted and this is observed for reduced frequencies higher than 0.1. However, the qualitative evolution of the 2D URANS hydrodynamic predictions is close enough to the experimental trend to provide useful physical insights.

The success of this first development phase of an oscillating-hydrofoils hydrokinetic turbine leads the way to the next step involving the deployment in a river or in a canal of a second generation prototype of increased power.

Mechanical losses associated to the coupling mechanism used in this first implementation are estimated to be a least 25% of the total power extracted. The next implementation will aim to reduce these losses and to use phase-shifted hydrofoils in order to uniformize the power production.

ACKNOWLEDGMENT

The authors gratefully acknowledge Le Fonds Québécois de la Recherche sur la Nature et les Technologies (FQRNT) for the funding of this research project through their team grant program.

The authors would also like to thank Natural Sciences and Engineering Research Council of Canada (NSERC) for partial financial support; La Société de Valorisation des Applications de la Recherche (SOVAR) for their interest and support; La Municipalité de Lac-Beauport for their collaboration and the access to their lake; the staff at Laval University mechanical engineering workshop for their excellent work on the turbine and boat machining and assembling; Marc-André Plourde Campagna for his active participation to this experimental campaign and colleagues at the laboratory LMFN for fruitful discussions and encouragements.

REFERENCES

[1] Bernitsas, M., Raghavan, K., Ben-Simon, Y., and E.M.H., G., 2008. "VIVACE (Vortex Induced Vibration Aquatic Clean Energy): A new concept in generation of clean and renewable energy from fluid flow". *ASME Journal of Offshore Mechanics and Arctic Engineering,* ***130***(4), November, p. 041101.

[2] Bernitsas, M., Ben-Simon, Y., Raghavan, K., and E.M.H., G., 2009. "The VIVACE Converter: Model tests at high damping and reynolds number around 10^5". *ASME Journal of Offshore Mechanics and Arctic Engineering,* ***131***(1), February, p. 011102.

[3] Bayandor, J., 2004. "Advanced zero head propulsion in review". In Proceedings of the ASME HT-FED04. Paper HT-FED04-56923.

[4] McKinney, W., and DeLaurier, J., 1981. "The wingmill: An oscillating-wing windmill". *Journal of Energy,* ***5***(2), pp. 109–115.

[5] Jones, K., Lindsey, K., and Platzer, M., 2003. "An investigation of the fluid-structure interaction in an oscillating-wing micro-hydropower generator". In *Fluid Structure Interaction II*, Chakrabarti, Brebbia, Almorza, and Gonzalez-Palma, eds. WIT Press, Southampton, UK, pp. 73–82.

[6] The Engineering Business Limited, 2002. Research and development of a 150 kw tidal stream generator. Tech. rep., Crown Copyright.

Copyright © 2010 by ASME

[7] The Engineering Business Limited, 2003. Stingray tidal energy device - phase 2. Tech. rep., The Engineering Business Limited.

[8] The Engineering Business Limited, 2005. Stingray tidal energy device - phase 3. Tech. rep., Crown Copyright.

[9] Incecik, A., Downie, M., and Okan, B., 2003. Modelling unsteady flow effects for the Stingray tidal generator. Tech. rep., Newcastle University. Confidential Report to Engineering Business, Report Number MT-2002-001.

[10] Pulse Tidal Limited, 2010. `http://www.pulsegeneration.co.uk`.

[11] Kinsey, T., and Dumas, G., 2008. "Parametric study of an oscillating airfoil in a power-extraction regime". *AIAA Journal,* ***46***(6), June, pp. 1318–1330.

[12] Kinsey, T., Dumas, G., and Olivier, M., 2007. "Heaving amplitude effects on oscillating wing turbines". In Proceedings of the 15th Annual Conference of the CFD Society of Canada. Paper CFD-2007-1068.

[13] Julien, S., Dumas, G., and Métivier, V., 2007. "URANS simulations of high amplitude flapping airfoils". In Proceedings of the 15th Annual Conference of the CFD Society of Canada. Paper CFD-2007-1117.

[14] Kinsey, T., 2010. "Analysis, optimization and demonstration of a new concept of hydrokinetic turbine based on oscillating hydrofoils". PhD thesis, Dept. of Mech. Eng., Laval University, Quebec City, Canada.

[15] Lalande, G., 2010. "Conception d'un prototype expérimental d'hydrogénérateur à ailes oscillantes". Master's thesis, Dept. of Mech. Eng., Laval University, Quebec City, Canada.

[16] ANSYS Inc., 2009. Ansys fluent 12.0 user's guide. `http://www.fluent.com`.

[17] Betz, A., and Prandtl, L., 1919. "Schraubenpropeller mit geringstem energieverlust". *Nacht. Ges. Wiss. Göttingen Math Phys.,* ***K1***, pp. 193–217.

[18] Newman, B., 1986. "Multiple actuator-disc theory for wind turbines". *Journal of Wind Engineering and Industrial Aerodynamics,* ***24***, pp. 215–225.

Copyright © 2010 by ASME